On the electroosmotic and MHD Jeffery–Hamel flow of Nano fluid influenced by wall slip conditions

Jacob Nagler

Jacob Nagler Graduated Bsc. (2011) and M.E. (2013) at the Technion, Faculty of Aerospace Engineering.

Affiliation: IAF & NIRC, Haifa, 34345, Israel.

(Received : 10.03.2016 ; Accepted : 05.04.2016)

ABSTRACT

Combined MHD and electroosmotic Jeffery–Hamel flow of Nano fluid type inside a wedge (inclined walls) with non-linear viscosity and wall friction are investigated analytically. As a result of similarity relations, one nonlinear ordinary differential equation is obtained and solved analytically with the appropriate assumptions $\left(f^2 \square\ f, 0 < \theta \le 20^0 \right)$. Moreover, excellent agreement was found between the obtained analytic solution and suggested simple parabolic approximation. Although it was found that in case where more effects are gradually being considered, a slight difference is emerged, but the most dramatic change between solutions occurs when solid to fluid ratio gets significant value. In addition, suitable match in the quantitatively and qualitatively aspects was found between literature results and obtained solution. In addition, analytical solution parametric investigation was performed for specific parameters choice. It was found that the normalized velocity was found to decrease gradually with the tangential direction progress and/or with friction coefficient increase. However, the normalized velocity profile gets higher values as long as the solid to fluid ratio increases. Additionally, Reynolds, Hartmann and solid volume fraction coefficient increase (separately or all together) have raised the normalized velocity function values. Finally, unprevail distinguished cases were introduced to understand flow complexity. It was found that the electrical field magnitude effect is significantly, especially for small friction coefficient values and for high wedge semi angle. Also, the combination between small friction coefficient values including small parameter flow values (Re and Ha numbers) and high electrically field may lead to un-optimized course of normalized velocity profile. The last case that was examined is concerned with friction coefficient variation effect on the normalized velocity profile for different values of wedge semi angle with high electric field for specific parameters choice. It was found that increasing friction coefficient leads to normalized velocity profile consolidation.

Keywords MHD; electroosmosis; Jeffery–Hamel flow; Nano fluid; slip conditions; friction; nonlinear ordinary differential equations; analytical solution; approximate solutions.

1 INTRODUCTION

Nano fluid mechanics interactions between various fluids type and different surfaces of various geometries have been investigated particularly during the last two decades. General theories on electro kinetic flows are being examined for more than six decades. For instance, in 1965 Rice and Whitehead [1] have presented their study on electro-kinetic flow in a narrow cylindrical capillary regarding the influence of the cylindrical capillary radius on electro-kinetic flow (Debye layer, interface potential). Moreover, nine years later, Sorensen and Koefoed [2] have introduced their study on electrokinetic effects in charged capillary tubes. They determined electrokinetic coefficients in a narrow tube filled with electrolyte solution and with a surface charge. Their model is suitable for stationary, laminar flow of Newtonian fluids under the validity of the linearized Poisson-Boltzmann equation. Their model solution is being coincided with Helmholtz solution in the limit region of the pores which are reported to be large enough compared with the Debye-Huckel length. One year later, Levine *et al*. [3] have published their study on electrokinetic flow in a narrow parallel-plate channel. Their flow model is composed of two charged walls of non-conducting, infinite parallel plates while the electrolyte has finite size. About three decades later in 2004, new phenomenon of ion enrichment/depletion connected to nano-channel structures has been discovered by Pu *et al*. [4]. They have found that after applying the voltage over the channel, ions are enriched quickly at the one end of the channel while depleted at the other end. Moreover, according their study, a direct link between enrichment/depletion and the extent of double-layer overlap does exist. Over the latter year, Plecis *et al*. [5] have proved the crucial influent of the electrostatic forces in nanofluidics by comparison between their analytical model and experiments. Strengthening the latter argument, analytical model of electrical double layer extension inside nano-channel with charged surfaces has been performed while resulting with the electrostatic exclusion of co-ions and enrichment in counterions, which affects the perm-selectivity of such structures. The authors [5] have demonstrated this phenomenon together with quantitative measurements of the ionic permeability change of Pyrex nano-slit at low ionic strength. They also state that the chemical examination of the Pyrex-water interface can be performed in less complex systems than the nano-slit. In addition, it was found that slit height parameter has an impact on the enrichment for small height values (thin channel) such as the channel should enable to reach higher perm-selectivity

**Corresponding Author*
e-mail: syanki@tx.technion.ac.il
Digital Object Identifier (DOI) : 10.2339/2016.19.4 555-568

for moderate ionic strength. Moreover, their model based on Poisson-Boltzmann equations can be applied in many aspects of biotechnological engineering and industry. It should be noted that according their study, the diffusive transport of charged species is valid whereas the concentration of is low enough compared to the bulk concentration. Two years later, Byun *et al*. [6] have published their study on electroosmosis based nanopipettor development. Their first version of their EO-driven nanopipettor pipe consists of a microfabricated EO pump, a polyacrylamide grounding interface and a nL-pL pipet-tip. According the study [6], good linear relationships between pipetted/dispensed volume and pipetting/dispensing time including the volume and the voltage applied to the pipettor has been obtained. However, the volume range that was applied in their study is from about 100 pL to about 300 nL, while it can be extended considerably. More details about volume range, pipetetting time and channel depth can be found in their study. One year later, new theory of thermodynamic efficiency optimization of an electroosmotic (EO) pump with a large surface area while being highly charged with nanoporous silica disk substrate was presented by Berrouche *et al*. [7]. The researchers have found that the optimum thermodynamic efficiency depends on the following parameters: temperature, silica zeta potential, viscosity, permittivity, ion valency, tortuosity of the nanoporous silica and mostly on the effective normalized pore radius of the substrate. Moreover, they found that by using de-ionized water as the pumping liquid, the optimized EO pump generates the maximum flow rate for specific pressure and under applied given voltage. During the same year, Chen *et al*. [8] have published their essay on new development of electroosmotic pump using nanosilica particles having an average size of 20-30 nm with packed capillary of a 5 cm x 530 mum. Another study from the same year was presented by Chen *et al*. [9]. Their study deals with electroosmotic pumping flow with high flow rate at low applied voltage using relatively thin alumina nano-porous membrane and uniform electric field caused by a contact of perpendicular platinum mesh electrode with the nano-channel inlet. They discovered that the flow rate values are usually high for low electrolyte (KCl) concentrations. In addition, flow rate drop occurs when concentration surpasses certain value. The latter study that was also published in the same year and provided by Seiler and Kirby [10] examines the computational modeling challenges of two dimensional fluid flow phenomenon governed by A/C electroosmosis in the micro and nano scales using COMSOL simulation program compared to numerical/analytical results. Initially, harmonic response of the ion flux with respect to the driving potential has been established and afterwards the Navier-Stokes application model was added. The model was solved and the A/C electroosmosis fluid flow was observed. Two years later, Ai *et al*. [11] have presented their study on the effects of electroosmotic flow on ionic current rectification in conical nanopores based on Nernst−Planck equations (ionic concentrations), the Poisson equation (electric potential) and Navier−Stokes equations (flow field). They informed that the preferential current direction of a negatively charged nanopore is toward the base (tip) under a relatively high ratio of the tip radius size to the Debye length while direction also changes with the charge polarity of the nanopore. In the same year, Piruska *et al*. [12] have published comprehensive review of Nanofluidics in chemical analysis. They emphasized the difference between nanofluidics and microfluidics systems including thoroughly discussion on chemical applications on various nano systems. Two years later, Aparajita and Satapathy [13] have presented a study on thermal transport analysis of combined electroosmotic and pressure-driven flow of power-law (shear-thinning and shear-thickening) nanofluids through a microchannel. They investigated the effect of different flow and electrolytic parameters on the thermal behavior of the flow under constant wall heat flux condition while taking into account the effects of viscous dissipation and Joule heating. Three nanofluidic parameters that have been taken into consideration are the viscosity, electrical permittivity and electrical resistivity. These parameters have been introduced as ratios with reference to the corresponding properties of a conventional fluid. On the one hand, they found that Nusselt number decreases with decreasing viscosity ratio and/or increasing permittivity ratio. On the other hand, Nusselt number increases with increasing resistivity ratio. Other distinguished studies from the same year of 2012 would be elaborated. The first study was presented by Avsec [14]. He has developed analytic model of nano-fluid motion including elektro-kinetic and electromagnetic forces together with heat transfer effects inside rectangular and circular micro-channels subjected to wall slip conditions. He has found that volume fraction of nano-particles has great influence on the velocity and also on the temperature distribution in the micro-channels. Second study was presented by Imani *et al*. [15] about Jeffery-hamel flow inside divergent channel and nano particles with high magnetic field using reconstruction of variational iteration method (RVIM) for solution. The latter study was performed by Kurtoğlu *et al*. [16]. Their study discusses the magnetic nano-particle suspensions and applications. The authors [16] claim that microscale technology permits the use of micropump while magnetically actuated ferro-fluids could have the potential to be used as an alternative micro pumping system. Last study that will be brought here and was published during 2012 is dealt with laminar, free convection boundary layer flow over a permeable isothermal truncated cone in the presence of a transverse magnetic field effect. A solution with suitable non-similarity analysis has been done by Ahmed and Mahdy [17] for the obtained one non-linear equation. The researchers have used different water

species based on nano-fluids while solving the problem by using fourth order Runge-Kutta with shooting technique (Ag-nanoparticles give a higher rate of heat transfer while TiO2 nanoparticles yield with the lowest value). Excellent agreement was found between vertical plate problem solutions and their study. Moreover, they found that solid volume fraction increase leads to the increase of the heat transfer rate whereas the skin fraction decreases. Additionally, the model of spherical nano-particles was found to be most beneficial in the context of heat transfer rate. Finally, magnetic field parameter increase results with decreasing of both of the velocity and local skin friction coefficient and in increase of the fluid temperature as well as the rate of heat transfer. One year later, similar study as Imani *et al*. [15] was published by Khidir [18]. A new modification of the standard homotopy perturbation method (HPM) including the Chebyshev pseudo spectral methods for solving nonlinear boundary value problems of Jeffery-Hamel flow with the magnetic field and nanoparticle effects is presented in his study [18]. He has shown good agreement between the suggested solution and other numerical solutions. Moreover, he proved that his solution method (SHPM) is more efficient and converges faster than the standard homotopy perturbation method. During his study, he found that increase of volume fraction causes an increase in the fluid velocity profile of diverging channels while the velocity decreases for the converging channels case. Moreover, he also found that the fluid velocity increases with increasing Hartman numbers for both diverging and converging channels cases. During 2013, numbers of distinguished studies of nano applications were emerged. For instance, Sadoughi *et al*. [19] have developed analytical method using reconstruction of variational iteration method (RVIM) based on Pade' approximation and Keller's box method in order to solve the non-linear two-dimensional forced convection boundary layer magneto hydro-dynamic (MHD) incompressible flow of AL2O3 nanofluid over a horizontal flat plate with variable magnetic field. Another study from the same year was performed by Umavathi and Shekar [20] and similarly by Ganji and Azimi [21]. They solved Jeffery-Hamel flow problem in the case of nanofluid with magnetic effect. Their solution is mainly based on a semi-numerical-analytical technique called differential transform method (DTM) together with comparative numerical analysis based on Runge-Kutta shooting method (RKSM). Both methods results have excellent agreement. Moreover, they found that Reynolds numbers increase leads to the velocity profile decrease and also increasing Hartmann number may lead to backflow reduction. In addition, they have shown that nano-particles cause to increase fluid velocity value. One year later in 2014, Hatami *et al*. [22] have published their study on Jeffery–Hamel MHD flow of nano-fluid through non-parallel walls by analytical analysis. They used Maxwell–Garnetts (MG) and Brinkman models for calculating the thermal conductivity and nano-fluid viscosity. They proved by comparison to other semi-analytical methods (DTM and DTM–Padé) that least square method is most accurate. Moreover, they have found that velocity boundary layer thickness decreases with the increase of Reynolds number and nanoparticle volume friction and it increases according to Hartmann number increase. However, the skin friction coefficient was found to be directly dependent on Reynolds number, opening angle and nanoparticle volume friction, while being increasing with these parameters but decreasing with Hartmann number. During the same year, Mao *et al*. [23] have also presented their study on electroosmotic flow (pumping) through a nanopore that traverses an insulating membrane. They have assumed low uniform density of surface charge on the membrane such as the linearized Poisson-Boltzmann equation can be used. The case of membrane with arbitrary thickness was solved numerically by solving the full Poisson–Nernst–Planck–Stokes system of equations using a finite volume method. Another study on MHD Jeffery-Hamel flow with nanoparticle by Hermite- Padé approximation was performed by Alam and Khan [24]. They examined the effects of nanoparticle and magnetic field on the nonlinear Jeffery-Hamel flow by perturbation method and Hermite-Padé approximation while comparing to Adomian decomposition method (ADM). They have discovered that Reynolds number increase leads to reduction of velocity near the walls. Additionally, Hartmann number increase may cause to backflow reduction while high value is being required to decline of backflow which are resulted due to large semi-cone angles or Reynolds numbers. They also obtained that momentum boundary layer thickness increases with increasing nano-particle volume fraction. Additional two more studies that were published during 2014 have been done by Nayak [25] and Deng *et al*. [26]. Nayak has developed solution to Poisson, Nernst--Planck and the Navier--Stokes equations in order to increase the mixing potential of ion species in micro and nano channels with heterogeneous surface potential involved with the discussion on the generation of vertical flow due to the presence of wall heterogeneity at different locations in the channel. He has found that strong recirculation vortices which appear above the heterogeneities generate a strong pressure gradient which increases the mixing performance. Deng *et al*. [26] have examined the problem of ion current rectification link to the concentration gradient of KCl solutions in polyethyleneimine modified glass nano-pipettes. One year later in 2015, the laminar axisymmetric flow of nanofluid over a non-linearly stretching sheet with the simultaneous effects of Brownian motion and thermophoretic diffusion of nanoparticles while no-slip boundary conditions were assumed, was presented and solved analytically using homotopy method by Mustafa *et al*. [27]. They have found that Brownian motion effect on the fluid temperature and wall heat transfer rate is insignificant.

Moreover, the nanoparticle volume fraction distribution was found to be negative near the vicinity of the stretching sheet. A study that combines thermal, electroosmotic, magnetic and pressure driven flow of nanofluids in microchannel into one problem was done by Ganguly & Sarkar *et al*. [28] using semi-analytical method. They have found that magneto-hydrodynamic effect reduces the transport of the liquid resulting in gradual reduction of heat transfer. Additionally, increase in nano-particle volume fraction leads to decrease in the rate of heat transfer. According [27]-[28], similar effects has been occurred with the increase in aggregate sizes of the nano-particles. Moreover, they also calculated the total entropy influence while it has been found to be highly effective at the thermally developing region where the nano-particles presence in the base fluid caused to reduction of the total entropy generation in the microchannel and therefore increasing nano-particle volume fraction where higher magnitude of total entropy generation has been observed near the channel walls region. The gradual increase in the liquid temperature with increase in Hartman number results in monotonically increasing values of the Nusselt number. However, at a particular value of Ha, with increasing nanoparticle volume fraction, Nu decreases indicating decrease in the heat transfer rate. Conical nanopore with the considering of electroosmotic flow (EOF) has been investigated analytically by solving a set of coupled Poisson, Nernst–Planck, and Navier–Stokes equations in the context of ionic current rectification (ICR) by Lin *et al*. [29]. During the same year, Laohakunakorn and Keyser [30] and also Moradi *et al*. [31] have presented studies on nano fluid while the first performed an experimental study on electroosmotic flows (EOFs) through conical nano-pores and the latter has made analytical study on the influence of heat transfer on the nonlinear Jeffery-Hamel flow problem in a nanofluid of three types of nano-particles (Cu, Al2O3, TiO2) by considering water as a base fluid in convergent/divergent channel, respectively. The solution was obtained by solving analytically (DTM) and numerically (Runge-Kutta) the nonlinear differential equation. Similarly, like former studies, the authors [30, 31] have found that the influence of solid volume fraction of the nano-particles on the heat transfer and fluid flow parameters is more pronounced when compared with the type of nano-particles. Moreover, they have also found that skin friction coefficient and Nusselt number for Al2O3 nano-fluid is highest in comparison to the other two nano-particles while the effect of solid volume fraction on the skin friction coefficient and Nusselt number in convergent and divergent channels are similar. On the other hand, the effects of fluid material parameters on skin friction coefficient and Nusselt number are opposite for the convergent and divergent channels.

The current essay develops and solves analytically and numerically EO and MHD Jeffery–Hamel flow of nano-fluid with wall slip conditions inside wedge channel based on the author previous studies on non-Newtonian Jeffery-Hamel flow wedge and in micro-channel [32], respectively. This essay continues the studies of Umavathi and Shekar [20], Alam and Khan [24] and Ganguly *et al*. [28].

2 PROBLEM FORMULATION MODEL

Consider a steady two-dimensional flow due to electrical source applied together with uniform magnetic field B of an incompressible conducting viscous fluid inside a wedge (non-parallel walls) with friction on the walls. The cylindrical polar coordinates (r,θ,z) have been selected to model the flow system as shown in Fig. 1 while the flow intersected in the z axis. It is assumed that the motion is purely radially dependent on r,θ only. Moreover, there are no changes with respect to z axis. The governing equations of motion will be elaborated here as follows. Equation of continuity can be written using Bird *et al*. [33] formulation as:

$$\nabla\cdot\mathbf{V}=0\rightarrow\frac{\rho_{nf}}{r}\frac{\partial}{\partial r}(ru_r)=0\,. \qquad (1)$$

while $\mathbf{V},\rho,u_r$ are the velocity vector, constant fluid density and the radial velocity vector, respectively.

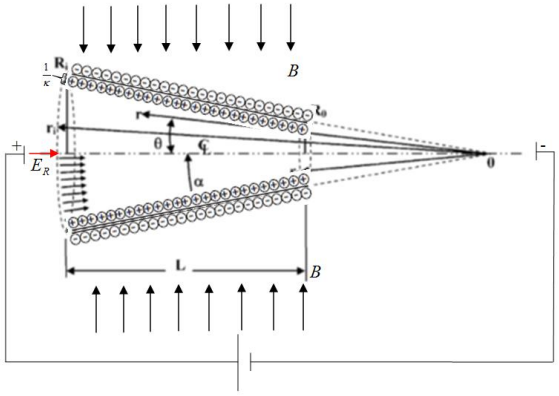

Fig. 1. Electro-magnetic wedge shape flow model illustration.

Now, the general equation of momentum can be written by:

$$\rho\left[\frac{\partial\mathbf{V}}{\partial t}+(\mathbf{V}\cdot\nabla)\mathbf{V}\right]=-\nabla\mathbf{p}+\nabla\cdot\boldsymbol{\tau}+F_B\,. \qquad (2)$$

while F_B and $\boldsymbol{\tau}$ are the body forces and stress vectors, respectively. Body forces are assumed to be generating according to electro-magnetic source ([20], [23], [28]). This source is a combination of Lorentz force (magnetic source) and electrostatic source (uniform electrical field in the radial direction), while gravitational body forces are negligible, based on [34] development, according to:

$$F_B=\sigma(\mathbf{E}+\mathbf{V}\times\mathbf{B})\times\mathbf{B}+F_r=-\left(\sigma B_0^{\,2}\cos\theta\sin\theta\hat{e}_\theta+\sigma B_0^{\,2}u_r\cos^2\theta\hat{e}_r\right)+\rho_e E_r \qquad (3)$$

where $\sigma,\mathbf{E},\mathbf{V},\mathbf{B},F_r$ are the constant electrical conductivity, induced electric field, fluid velocity

vector, external magnetic field and the electrical force, respectively. Lorentz force is created due to the flow of a conductive fluid under the influence of a uniform magnetic field. According to Faraday's law, eddy currents are generated by electromotive force due to conductive fluid movement through a magnetic field. As introduced by Thess [35] eddy current creates induced magnetic field based on Ampère's law. The interaction between eddy currents and the total magnetic field results with the opposite Lorentz force (against flow direction). The magnetic force is composed of the magnetic field $\mathbf{B}$ with constant magnetic induction strength B_0, which is being applied in the transverse direction of the flowing fluid along unidirectional fully developed electroosmotic flow velocity u_r. Moreover, assuming that the magnetic Reynolds number is sufficiently small, then the induced magnetic and electric fields can be neglected. In addition, since there are no electrical fields in the z axis direction (inside the sheet) only in the radial electric field, than no magnetic force can be generated in the $\left(\hat{r},\theta\right)$ directions out of the forces mentioned in Eqs. (2)-(3). According to Ganguly *et al*. [28], the electroosmosis driving force part is induced by the interaction of an applied electric field in the nano-fluid effective kinematic viscosity, the nano-fluid effective density, the base fluid density and the solid particles density, respectively. Integrative systems that combine between electric and magnetic forces including thermal effects are discussed by ([28], [36]). The Navier-Stokes equations in polar coordinates form ([20] - [21], [24]) are:

while the momentum equations are derived by using the fully cylindrical coordinates flow as developed by Membrado and Pacheco [37]. One step before completing the model formulation is to determine the net charge density ρ_e. Using Poisson equation together with analogy comprehension with Ganguly *et al*. [28] studies, the following equation for the net charge is obtained in the tangential direction which is perpendicular to the wedge wall (in Cartesian coordinates it is represented in the perpendicular y direction):

$$\rho_e(\theta) = -\kappa^2 \varepsilon \psi_w \frac{\cosh(\kappa\theta)}{\cosh(\kappa\alpha)} \tag{9}$$

according to $\frac{\partial^2\psi}{\partial\theta^2} = -\frac{\rho_e}{\varepsilon}, \psi_{(\theta=\alpha)} = \psi_w, \frac{\partial\psi}{\partial\theta}_{(\theta=0)} = 0$. While κ is defined as Debye length and is calculated by

$$\hat{r}:\ \rho_{nf}u_r\frac{\partial u_r}{\partial r} = -\frac{\partial P}{\partial r} - \left[\frac{1}{r}\frac{\partial}{\partial r}\left(r\tau_{rr}\right) + \frac{1}{r}\frac{\partial\tau_{r\theta}}{\partial\theta} - \frac{\tau_{\theta\theta}}{r}\right] + F_r$$
$$\rho_{nf}u_r\frac{\partial u_r}{\partial r} = -\frac{\partial P}{\partial r} + 2\frac{\partial\mu_{nf}}{\partial r}\frac{\partial u_r}{\partial r} + \frac{1}{r^2}\frac{\partial\mu_{nf}}{\partial\theta}\frac{\partial u_r}{\partial\theta} + \mu_{nf}\left[\frac{\partial^2 u_r}{\partial r^2} + \frac{1}{r^2}\frac{\partial^2 u_r}{\partial\theta^2} + \frac{1}{r}\frac{\partial u_r}{\partial r} - \frac{u_r}{r^2}\right] - \sigma B_0^2 u_r\cos^2\theta + \rho_e E_r \tag{4}$$

while shear rate components behave according the assumptions that $u_\theta = u_z = 0,\ \frac{\partial(\ )}{\partial z} = 0$:

$$\tau_{rr} = -p + 2\mu_{nf}\frac{\partial u_r}{\partial r}, \tau_{\theta\theta} = -p + 2\mu_{nf}\frac{u_r}{r}, \tau_{r\theta} = \frac{\mu_{nf}}{r}\frac{\partial u_r}{\partial\theta}. \tag{5}$$

The equation of momentum in the tangential axis is:

$$\hat{\theta}: -\frac{1}{\rho_{nf}r}\frac{\partial P}{\partial\theta} - \left[\frac{1}{r^2}\frac{\partial}{\partial r}\left(r^2\tau_{r\theta}\right) + \frac{1}{r}\frac{\partial\tau_{\theta\theta}}{\partial\theta}\right] = 0$$
$$\frac{1}{\rho_{nf}r}\frac{\partial P}{\partial\theta} - \frac{1}{\rho_{nf}r}\frac{\partial\mu_{nf}}{\partial r}\frac{\partial u_r}{\partial\theta} - \frac{2}{\rho_{nf}r^2}\frac{\partial\mu_{nf}}{\partial\theta}u_r - \frac{2\nu_{nf}}{r^2}\frac{\partial u_r}{\partial\theta} + u_r\frac{\sigma B_0{}^2}{\rho_{nf}}\cos\theta\sin\theta = 0 \tag{6}$$

the radial direction E_r and the net charge density ρ_e in the EDL (electric double layer). The viscosity term is expressed using the following components [28]:

$$\mu_{nf} = \frac{\mu_f}{(1-\phi)^{2.5}}, \nu_{nf} = \frac{\mu_{nf}}{\rho_{nf}}, \rho_{nf} = \rho_f(1-\phi) + \rho_s\phi. \tag{8}$$

While $\phi, \nu_{nf}, \rho_{nf}, \rho_f, \rho_s$ are the solid volume fracture, $\kappa^{-1} = \sqrt{\varepsilon k_B T \big/ 2e^2 z^2 n_\infty}$, where n_∞ and z are the bulk number concentration and the valence of ions, respectively. ε, e, k_B, T are the electric permittivity, elementary charge, Boltzmann constant and the absolute temperature, respectively. Additionally, κR_o is

$$-\frac{1}{\rho_{nf}}\frac{\partial P}{\partial r} + \frac{2}{\rho_{nf}}\frac{\partial\mu_{nf}}{\partial r}\frac{\partial u_r}{\partial r} + \frac{1}{\rho_{nf}r^2}\frac{\partial\mu_{nf}}{\partial\theta}\frac{\partial u_r}{\partial\theta} + \nu_{nf}\left[\frac{\partial^2 u_r}{\partial r^2} + \frac{1}{r^2}\frac{\partial^2 u_r}{\partial\theta^2} + \frac{1}{r}\frac{\partial u_r}{\partial r} - \frac{u_r}{r^2}\right] - \frac{\sigma B_0^2}{\rho_{nf}}u_r\cos^2\theta - \kappa^2\varepsilon\psi_w\frac{\cosh(\kappa\theta)}{\cosh(\kappa\alpha)}\frac{E_r}{\rho_{nf}} - u_r\frac{\partial u_r}{\partial r} = 0 \tag{7}$$

the electrokinetic parameter that represents the ratio of the half channel height (change with angle and radius) to the EDL thickness. Hence, after inserting equation (8) into (5), we have:

With the appropriate slip boundary conditions as follows:

$$\frac{\partial u}{\partial \theta}(\theta = \pm\alpha) = \mp m u(\theta) \tag{11}$$

while $m \geq 0$ is the friction coefficient factor. These conditions represent the relative slip friction between the fluid and the wall. On the one hand, a smooth boundary is described by $m = 0$. On the other hand, perfectly rough wall is obtained for $m = 1$. It is based on recent research studies about Mises effective stress and attributed to both Tresca and Prandtl. Similar studies on wall friction condition (12) are available for a variety of non-Newtonian fluids like elasto-viscoplastic and structural fluids [32], [38]. A third condition is joined to the other two conditions (13), which supplements [32]:

$$Q = \int_{(A)} u_r dA = -\int_{-\alpha}^{\alpha} u_r r d\theta \tag{15}$$

while A represents the cross sectional radial surface area of the flow field with the element area $dA = rd\theta$, within the deformation zone. α represents the wedge semi angle where flow field domain is confined between two rigid rough smoothing walls ($\theta = \pm\alpha$) that enables slip condition. Q is the steady state planar flow rate. In order to simplify the model, the following transformation will be applied using relation (1) as shown in Fig. 1:

$$u_r = -Q\frac{f(\theta)}{r} \tag{16}$$

Differentiating equation (9) along the tangential direction leads to:

$$-\frac{1}{\rho_{nf}}\frac{\partial^2 P}{\partial r\partial\theta}+\frac{2}{\rho_{nf}}\frac{\partial^2\mu_{nf}}{\partial r\partial\theta}\frac{\partial u_r}{\partial r}+\frac{2}{\rho_{nf}}\frac{\partial\mu_{nf}}{\partial r}\frac{\partial^2 u_r}{\partial r\partial\theta}+\frac{1}{\rho_{nf}r^2}\frac{\partial^2\mu_{nf}}{\partial\theta^2}\frac{\partial u_r}{\partial\theta}+\frac{1}{\rho_{nf}r^2}\frac{\partial\mu_{nf}}{\partial\theta}\frac{\partial^2 u_r}{\partial\theta^2}+\frac{1}{\rho_{nf}}\frac{\partial\mu_{nf}}{\partial\theta}\left[\begin{matrix}\frac{\partial^2 u_r}{\partial r^2}+\frac{1}{r^2}\frac{\partial^2 u_r}{\partial\theta^2}\\ +\frac{1}{r}\frac{\partial u_r}{\partial r}-\frac{u_r}{r^2}\end{matrix}\right]+\nu_{nf}\left[\begin{matrix}\frac{\partial^3 u_r}{\partial r^2\partial\theta}+\frac{1}{r^2}\frac{\partial^3 u_r}{\partial\theta^3}+\\ \frac{1}{r}\frac{\partial^2 u_r}{\partial r\partial\theta}-\frac{1}{r^2}\frac{\partial u_r}{\partial\theta}\end{matrix}\right] \tag{10}$$

$$-\frac{\sigma B_0^2}{\rho_{nf}}\frac{\partial u_r}{\partial\theta}\cos^2\theta+\frac{\sigma B_0^2}{\rho_{nf}}u_r\sin 2\theta-\frac{\kappa^3\varepsilon\psi_w E_r}{\rho_{nf}\cosh(\kappa\alpha)}\sinh(\kappa\theta)-\frac{\partial u_r}{\partial\theta}\frac{\partial u_r}{\partial r}-u_r\frac{\partial^2 u_r}{\partial r\partial\theta}=0$$

Multiplying equation (7) by r together with differentiation performance along the radial direction yields:

$$\frac{1}{\rho_{nf}}\frac{\partial^2 P}{\partial r\partial\theta}-\frac{1}{\rho_{nf}}\frac{\partial^2\mu_{nf}}{\partial r^2}\frac{\partial u_r}{\partial\theta}-\frac{1}{\rho_{nf}}\frac{\partial\mu_{nf}}{\partial r}\frac{\partial^2 u_r}{\partial r\partial\theta}-\frac{2}{\rho_{nf}r}\frac{\partial^2\mu_{nf}}{\partial r\partial\theta}u_r+\frac{2}{\rho_{nf}r^2}\frac{\partial\mu_{nf}}{\partial\theta}u_r-\frac{2}{\rho_{nf}r}\frac{\partial\mu_{nf}}{\partial\theta}\frac{\partial u_r}{\partial r}-\ldots \tag{11}$$

$$-\frac{2\nu_{nf}}{r}\frac{\partial^2 u_r}{\partial r\partial\theta}+\frac{2\nu_{nf}}{r^2}\frac{\partial u_r}{\partial\theta}-\frac{2}{\rho_{nf}r}\frac{\partial\mu_{nf}}{\partial r}\frac{\partial u_r}{\partial r}+u_r\frac{\sigma B_0^{\,2}}{2\rho_{nf}}\sin 2\theta+\frac{\partial u_r}{\partial r}\frac{\sigma B_0^{\,2}}{2\rho_{nf}}r\sin 2\theta=0$$

Therefore by adding equation (11) to equation (10), the following nonlinear differential equation is obtained:

$$\frac{2}{\rho_{nf}}\frac{\partial^2\mu_{nf}}{\partial r\partial\theta}\frac{\partial u_r}{\partial r}+\frac{1}{\rho_{nf}}\frac{\partial\mu_{nf}}{\partial r}\frac{\partial^2 u_r}{\partial r\partial\theta}+\frac{1}{\rho_{nf}r^2}\frac{\partial^2\mu_{nf}}{\partial\theta^2}\frac{\partial u_r}{\partial\theta}+\frac{1}{\rho_{nf}r^2}\frac{\partial\mu_{nf}}{\partial\theta}\frac{\partial^2 u_r}{\partial\theta^2}+\frac{1}{\rho_{nf}}\frac{\partial\mu_{nf}}{\partial\theta}\left[\frac{\partial^2 u_r}{\partial r^2}+\frac{1}{r^2}\frac{\partial^2 u_r}{\partial\theta^2}-\frac{1}{r}\frac{\partial u_r}{\partial r}+\frac{u_r}{r^2}\right] \tag{12}$$

$$+\nu_{nf}\left[\frac{\partial^3 u_r}{\partial r^2\partial\theta}+\frac{1}{r^2}\frac{\partial^3 u_r}{\partial\theta^3}-\frac{1}{r}\frac{\partial^2 u_r}{\partial r\partial\theta}+\frac{1}{r^2}\frac{\partial u_r}{\partial\theta}\right]-\frac{2}{\rho_{nf}r}\frac{\partial^2\mu_{nf}}{\partial r\partial\theta}u_r-\frac{2}{\rho_{nf}r}\frac{\partial\mu_{nf}}{\partial r}\frac{\partial u_r}{\partial r}-\frac{\partial u_r}{\partial\theta}\frac{\partial u_r}{\partial r}-u_r\frac{\partial^2 u_r}{\partial r\partial\theta}-\frac{1}{\rho_{nf}}\frac{\partial^2\mu_{nf}}{\partial r^2}\frac{\partial u_r}{\partial\theta}-\frac{\sigma B_0^2}{\rho_{nf}}\frac{\partial u_r}{\partial\theta}\cos^2\theta+\ldots$$

$$+3\frac{\sigma B_0^2}{2\rho_{nf}}u_r\sin 2\theta+\frac{\partial u_r}{\partial r}\frac{\sigma B_0^{\,2}}{2\rho_{nf}}r\sin 2\theta-\frac{\kappa^3\varepsilon\psi_w E_r}{\rho_{nf}\cosh(\kappa\alpha)}\sinh(\kappa\theta)=0$$

Thus the nonlinear differential equation (12) takes the following form after substituting (15) and dividing it by the density ρ_{nf}:

$$\frac{2Q}{\rho_{nf}r^2}\frac{\partial^2\mu_{nf}}{\partial r\partial\theta}f+\frac{Q}{\rho_{nf}r^2}\frac{\partial\mu_f}{\partial r}f'-\frac{Q}{\rho_{nf}r^3}\frac{\partial^2\mu_{nf}}{\partial\theta^2}f'-\frac{Q}{\rho_{nf}r^3}\frac{\partial\mu_{nf}}{\partial\theta}f''-\frac{1}{\rho_{nf}}\frac{\partial\mu_{nf}}{\partial\theta}\left[\frac{Q}{r^3}f''+\frac{4Q}{r^3}f\right]-\nu_{nf}\left[\frac{4Q}{r^3}f'+\frac{Q}{r^3}f'''\right]+\ldots \tag{12}$$

$$+\frac{2Q}{\rho_{nf}r^2}\frac{\partial^2\mu_{nf}}{\partial r\partial\theta}f-\frac{2Q}{\rho_{nf}r^3}\frac{\partial\mu_{nf}}{\partial r}f+2\frac{Q^2}{r^3}ff'+\frac{Q}{\rho_{nf}r}\frac{\partial^2\mu_{nf}}{\partial r^2}f'+\frac{Q\sigma B_0^{\,2}}{\rho_{nf}r}f'\cos^2\theta-Q\frac{\sigma B_0^{\,2}}{\rho_{nf}r}f\sin 2\theta-\frac{\kappa^3\varepsilon\psi_w E_r}{\rho_{nf}\cosh(\kappa\alpha)}\sinh(\kappa\theta)=0$$

Applying the assumption of constant fluid viscosity $\mu_{nf} = \text{constant}$ which means that also $\mu_f = \text{constant}$ according to (4), leads to the following non-linear differential equation:

$$2\frac{Q^2}{r^3}ff'-\nu_{nf}\left[\frac{4Q}{r^3}f'+\frac{Q}{r^3}f'''\right]+\frac{Q\sigma B_0^{\,2}}{\rho_{nf}r}f'\cos^2\theta-\frac{Q}{r}\frac{\sigma B_0^{\,2}}{\rho_{nf}}f\sin 2\theta-\frac{\kappa^3\varepsilon\psi_w E_r}{\rho_{nf}\cosh(\kappa\alpha)}\sinh(\kappa\theta)=0 \tag{13}$$

Multiplying Eq. (17) by r^3 and dividing it by Q and ν_{nf}, yields:

$$f'''+4f'-2\,\mathrm{Re}(1-\phi)^{2.5}\left[(1-\phi)+\frac{\rho_s}{\rho_f}\phi\right]ff'-Ha\left(f'\cos^2\theta-f\sin 2\theta\right)(1-\phi)^{1.25}+c_1\sinh(\kappa\theta)=0 \tag{14}$$

Where $c_1 = \frac{\varepsilon \psi_w E_r (\kappa r)^3}{\kappa Q \cosh(\kappa\alpha)\mu_f}$. In addition, Reynolds and Hartmann numbers are defined ([34]) by $Ha = (B_0 r)^2 \frac{\sigma}{\mu_f}, \mathrm{Re} = \frac{Q\rho_f}{\mu_f}$, respectively. Note that c_1 and Ha numbers are dependent on r. In order to cancel this dependency and to have similarity solutions which dependent only on the wedge semi angle θ one can assume that E_r or ψ_w or $\varepsilon \propto \frac{1}{r^3}$ and B_0 or $\sigma \propto \frac{1}{r^2}$. Accordingly,

$$Ha = \frac{\sigma_0 B_0^{\,2}}{\mu_f}, c_1 = \frac{\varepsilon_0 \psi_w E_r \kappa^2}{Q\cosh(\kappa\alpha)\mu_f} \tag{17}$$

While σ_0, ε_0 are constants. Integrating Eq. (18) along θ direction leads to the following equilibrium:

$$f'' + \left[4 - Ha(1-\phi)^{1.25}\cos^2\theta\right] f - 2\,\mathrm{Re}(1-\phi)^{2.5}\left[(1-\phi) + \frac{\rho_s}{\rho_f}\phi\right] f^2 + c_1\cosh(\kappa\theta) = d \tag{18}$$

with $\int f'\cos^2\theta - f\sin 2\theta d\theta = f\cos^2\theta, \cosh(\kappa\theta) = \frac{e^{\kappa\theta} + e^{-\kappa\theta}}{2}$ and d is the integration constant. Rearrangement of equation (20) members leads to one non differential equation which depends only on θ:

$$f'' + \left[4 - Ha(1-\phi)^{1.25}\cos^2\theta\right] f - 2\,\mathrm{Re}(1-\phi)^{2.5}\left[(1-\phi) + \frac{\rho_s}{\rho_f}\phi\right] f^2 = d - c_1\frac{e^{\kappa\theta} + e^{-\kappa\theta}}{2} \tag{19}$$

Based on previous studies, equation (21) can be treated as particular case of the general equation obtained by the author (Nagler – observe equation no. 25 there, [32]). In this stage we will try to solve Eq. (21) analytically. Suppose that $f^2 \propto f$ and $0 < \theta \le 20^0$, then Eq. (21) will behave according the following form:

$$f'' + \left(4 - HaJ_2 - 2J_1\right) f = d - c_1\frac{e^{\kappa\theta} + e^{-\kappa\theta}}{2}, \tag{20}$$

While

$$\cos^2\theta \propto 1, J_1 = 2(1-\phi)^{2.5}\,\mathrm{Re}\left[(1-\phi) + \frac{\rho_s}{\rho_f}\phi\right], J_2 = (1-\phi)^{1.25}. \tag{21}$$

Equation (22) solution will be done by two stages – homogenous and particular, according to:

$$f_h = \begin{cases} a_1 e^{\sqrt{4 - HaJ_2 - 2J_1}\theta} + a_2 e^{-\sqrt{4 - HaJ_2 - 2J_1}\theta}, 4 - HaJ_2 - 2J_1 > 0 \\ a_1\cos\left(\sqrt{4 - HaJ_2 - 2J_1}\theta\right) + a_2\sin\left(\sqrt{4 - HaJ_2 - 2J_1}\theta\right), 4 - HaJ_2 - 2J_1 < 0 \end{cases}. \tag{22}$$

While a_1, a_2 are constants. The particular solution of equation (22) is:

$$f_p = \frac{d}{4 - HaJ_2 - 2J_1} - \frac{c_1}{2}\frac{e^{\kappa\theta} + e^{-\kappa\theta}}{4 - HaJ_2 - 2J_1 + \kappa^2} \tag{23}$$

The final approximate solution for small values of wedge semi angle over the range $0^0 < \theta \le 20^0$ is

$$f = f_h + f_p = \begin{cases} \text{IF } 4 - HaJ_2 - 2J_1 > 0: \\ a_1 e^{\sqrt{4 - HaJ_2 - 2J_1}\theta} + a_2 e^{-\sqrt{4 - HaJ_2 - 2J_1}\theta} + \frac{d}{4 - HaJ_2 - 2J_1} - \frac{c_1}{2}\frac{e^{\kappa\theta} + e^{-\kappa\theta}}{4 - HaJ_2 - 2J_1 + \kappa^2} \\ \text{IF } 4 - HaJ_2 - 2J_1 < 0: \\ a_1\cos\left(\sqrt{4 - HaJ_2 - 2J_1}\theta\right) + a_2\sin\left(\sqrt{4 - HaJ_2 - 2J_1}\theta\right) + \frac{d}{4 - HaJ_2 - 2J_1} - \frac{c_1}{2}\frac{e^{\kappa\theta} + e^{-\kappa\theta}}{4 - HaJ_2 - 2J_1 + \kappa^2} \end{cases} \tag{24}$$

Now, in order to determine the constants a_1, a_2 and d, the following transformed conditions (13) – (14) should be applied on relation (26) according to:

$$f'(\theta = \pm\alpha) = \mp m f(\theta = \pm\alpha) \text{ or } \begin{cases} f'(\alpha) = -m f(\alpha) \\ f'(0) = 0 \end{cases} \tag{25}$$

Due to flow field symmetry assumption, both conditions can simply be written by the right column. The normalized transformed flow rate condition (14) is in the form:

$$\int_{-\alpha}^{\alpha} f d\theta = 1 \tag{26}$$

Hence, the final solution coefficients are:

$$\text{IF } 4-HaJ_2-2J_1>0:$$

$$a_1=a_2=-\frac{m\left(\frac{d}{T_1^2}-T_5\right)-\frac{\kappa c_1}{2}T_2}{mT_4+T_1T_3},d=\left(\frac{1}{2}+\frac{T_2c_1}{4\kappa}-\frac{mT_5+\frac{\kappa}{2}c_1T_2}{mT_4+T_1T_3}\frac{T_3}{T_1}\right)\left(\frac{\alpha}{T_1^2}-\frac{m/T_1^2}{mT_4+T_1T_3}\frac{T_3}{T_1}\right)^{-1} \tag{27}$$

$$\text{IF } 4-HaJ_2-2J_1<0:$$

$$a_1=\frac{\frac{\kappa c_1}{2}T_2-m\left(\frac{d}{T_1}-T_5\right)}{m\cos\left(T_1\alpha\right)-T_1\sin\left(T_1\alpha\right)},a_2=0,d=\frac{\frac{T_1^2}{2\alpha}\left(1+\frac{T_2c_1}{2\kappa}\right)-\frac{\kappa c_1T_2+2mT_5}{2T_6\alpha}T_1\sin\left(T_1\alpha\right)}{1+\frac{m}{T_1T_6\alpha}\sin\left(T_1\alpha\right)}$$

Where,

$$T_1=\sqrt{4-HaJ_2-2J_1},T_2=\frac{e^{\kappa\alpha}-e^{-\kappa\alpha}}{T_1^2+\kappa^2},T_3=e^{T_1\alpha}-e^{-T_1\alpha},T_4=e^{T_1\alpha}+e^{-T_1\alpha},T_5=\frac{c_1}{2}\frac{e^{\kappa\alpha}+e^{-\kappa\alpha}}{T_1^2+\kappa^2}, \tag{28}$$

$$T_6=m\cos\left(T_1\alpha\right)-T_1\sin\left(T_1\alpha\right)$$

Suggested functions based on the author relevant mathematical knowledge on micro fluid flow [32] will be introduced here. Parabolic approximation which fulfills boundary conditions (27)-(28) is brought as follows [32]:

$$f_1(\theta)\approx b_1\left(1-b_2\theta^2\right)=\frac{1-\frac{m}{2\alpha+m\alpha^2}\theta^2}{2\alpha-\frac{2}{3}\frac{m\alpha^3}{2\alpha+m\alpha^2}}=\frac{2\alpha+m\alpha^2-m\theta^2}{4\alpha^2+\frac{4}{3}m\alpha^3} \tag{31}$$

$$b_1=\frac{1}{2\alpha-2b_2\frac{\alpha^3}{3}}=\frac{1}{2\alpha-\frac{2}{3}\frac{m\alpha^3}{2\alpha+m\alpha^2}},b_2=\frac{m}{2\alpha+m\alpha^2}$$

while $\alpha\neq 0$.

In the next section, comparison will be performed and discussed between approximate analytical solutions and literature results.

3 RESULTS & DISCUSSION

In this section parametric investigation based on Eq. (29) through illustrative results will be presented and discussed. Initially, suppose that the following parameters are considered

$$\alpha=2.5^0,\phi=0,\mathrm{Re}=250,\kappa=1000\left[\frac{1}{nm}\right],Ha=50,\frac{\rho_s}{\rho_f}=10^4,\psi_w=-50[mV],E=30[\frac{\mathrm{kV}}{m}],\varepsilon_0=-8.85\cdot10^{-12}\left[\mathrm{F/m}\right].$$

Seemingly, the normalized velocity (f) was found to decrease gradually with the tangential direction progress as appear in Fig. 1. Moreover, friction coefficient (m) increase leads to normalized velocity profile values decrease as shown in Fig. 1. Many studies are usually using the no-slip boundary condition. Here, the case where friction coefficient (m) value becomes large enough to represent "infinity" is for $m=10^6$ and condition (27) becomes $f(\alpha)=0$. The obtained solution has full compatibility with [24], [28] and Dib *et al*. [39]. The opposite extreme case where $m=0$ or $f'(\alpha)=0$ is illustrated in Fig. 2 by horizontal line parallel to the θ axis while good agreement has been achieved [32]. Further explanation for this phenomenon will be brought in the next section. However, increase of wedge semi angle value leads to increase of the normalized velocity profile as appear in Fig. 3. Concentrating on the solid to fluid ratio ρ_s/ρ_f teaches us that the normalized velocity profile gets higher value as long as the fracture increases as illustrated in Fig. 4. Initial observation at two distinguished characteristics of the flow: Reynolds (Re) and Hartmann (Ha) numbers show that an increase in these numbers raises the normalized velocity function values as shown in Figs. 5-6. In addition, solid volume fraction coefficient (ϕ) increase is accompanied with normalized velocity profile result increase.

Next, the discussion will revolve around the comparison between the approximate analytical solution (29) and suggested approximate parabolic solution (31). In case where flow effects (including inertia, magnetic, electrically, etc.) can be neglected, both solutions are coincided for each value of the wedge semi angle and friction coefficient as illustrated in Fig. 7. (a-b), respectively. In case where more effects are gradually being considered, a slight difference is emerged, but the most dramatic change between solutions occurs when solid to fluid ratio ρ_s/ρ_f gets significant value as shown in Fig. 9.

Next section will discuss on the influence of small friction coefficient values through special cases.

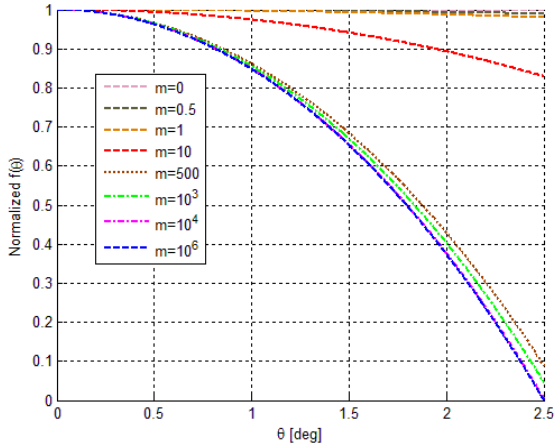

Fig. 2. Normalized velocity $f(\theta)$ for various values of friction coefficient (m) while

$\alpha = 2.5^0, \phi = 0, \mathrm{Re} = 250, \kappa = 1000\left[\frac{1}{nm}\right], Ha = 50, \frac{\rho_s}{\rho_f} = 10^4$.

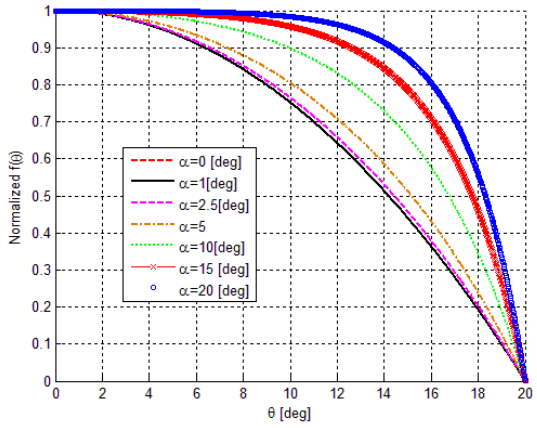

Fig. 3. Normalized velocity $f(\theta)$ for various values of semi wedge angle (α) while

$\phi = 0, \mathrm{Re} = 250, \kappa = 1000\left[\frac{1}{nm}\right], Ha = 50, \frac{\rho_s}{\rho_f} = 10^4, m = 10^6$.

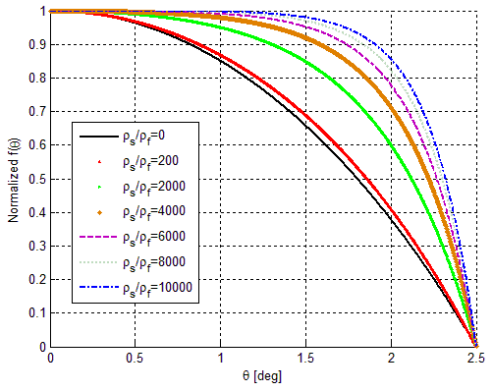

Fig. 4. Normalized velocity $f(\theta)$ for various values of solid to fluid fraction coefficient ρ_s / ρ_f while

$\alpha = 2.5^0, \phi = 0.01, \mathrm{Re} = 250, \kappa = 1000\left[\frac{1}{nm}\right], Ha = 50, m = 10^6$

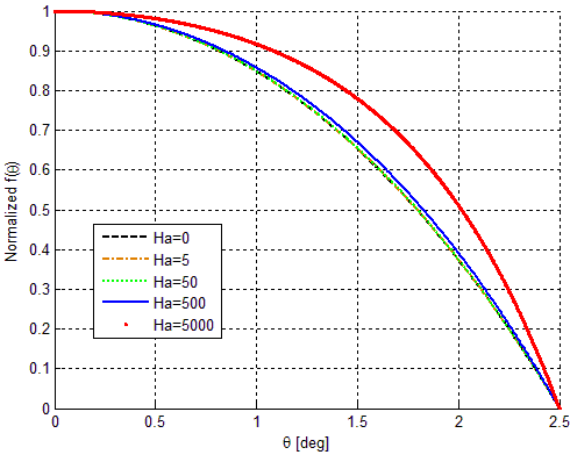

Fig. 5. Normalized velocity $f(\theta)$ for various values of Hartman number (Ha) while

$\alpha = 2.5^0, \phi = 0, \mathrm{Re} = 250, \kappa = 1000\left[\frac{1}{nm}\right], m = 10^6, \frac{\rho_s}{\rho_f} = 10^4$.

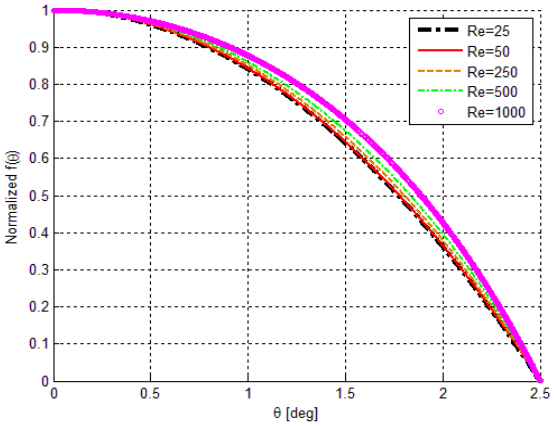

Fig. 6. Normalized velocity $f(\theta)$ for various values of Reynolds number (Re) while

$\alpha = 2.5^0, \phi = 0, Ha = 50, \kappa = 1000\left[\frac{1}{nm}\right], m = 10^6, \frac{\rho_s}{\rho_f} = 10^4$.

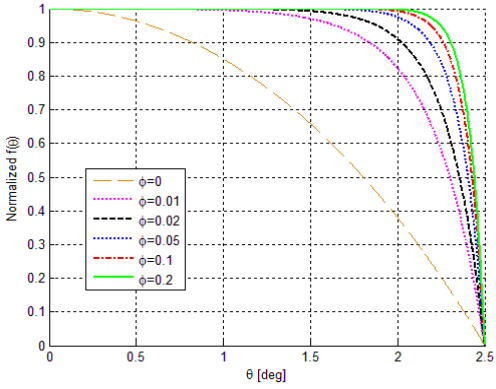

Fig. 7. Normalized velocity $f(\theta)$ for various values of solid volume fraction (ϕ)

while $\alpha = 2.5^0, \mathrm{Re} = 250, Ha = 50, \kappa = 1000\left[\frac{1}{nm}\right], m = 10^6, \frac{\rho_s}{\rho_f} = 10^4$

Suppose that $\alpha = 20^0, \phi = 0, \mathrm{Re} = 0, \kappa = 1000\left[\frac{1}{nm}\right], Ha = 0, \frac{\rho_s}{\rho_f} = 0, \psi_w = -50[mV]$

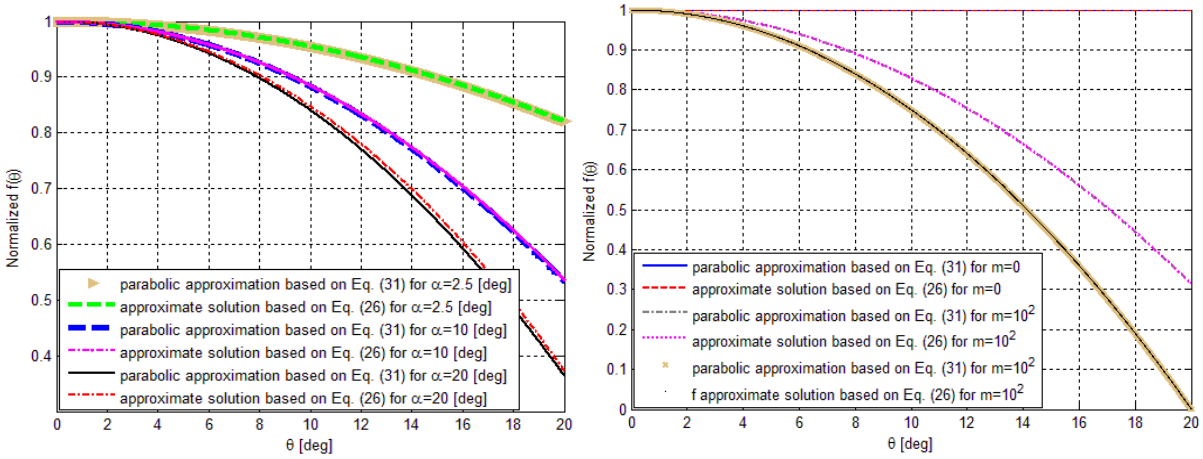

Fig. 8. Normalized velocity $f(\theta)$ comparison between Eqs. (29) and (31) for various values of a. wedge semi angle (α) while $m = 10^1$. where $\phi = 0,\ \mathrm{Re} = 0, \kappa = 1000\left[\frac{1}{nm}\right], Ha = 0, \frac{\rho_s}{\rho_f} = 0$ .b. friction coefficient (m) while

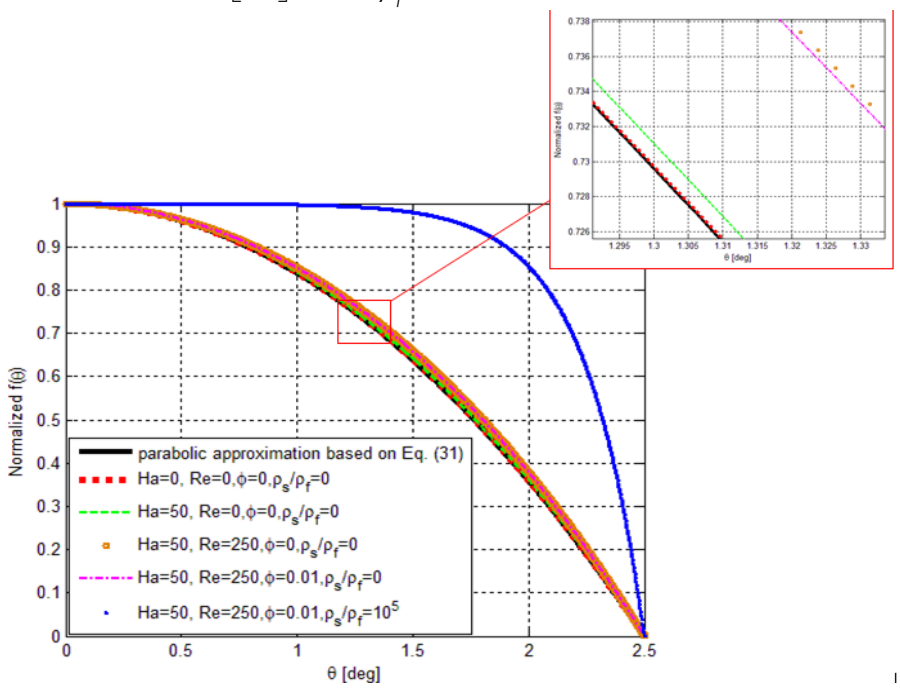

Fig. 9. Normalized velocity $f(\theta)$ comparison between Eqs. (29) and (31) based on gradual parametric variation (evolution) while $\alpha = 2.5^0, m = 10^6$ are constants through process.

4 DISTINGUISH FLUID BEHAVIOR EXAMINATION DUE TO SMALL FRICTION COEFFICIENT VALUES

In this section three unprevail distinguished cases will be brought for discussion. These cases represent the fluid mechanics complexity and may be used for further future studies investigations. Firstly, the case where friction coefficient becomes zero will be analyzed. . As a result of substitution into Eq. (29), the horizontal line is slightly varied with the electrical field as shown in Fig. 10. In conclusion, the increase of the electrical field causes to the normalized velocity to decrease slightly gradually while the wedge semi angle was chosen to obtain maximum value $\left(\alpha = 20^0\right)$ such as this phenomenon will be identified clearly. The second

phenomenon that will be introduced shows that for specific parameters choice

$$\left(m=0.5,\phi=0.03,\mathrm{Re}=25,\kappa=1000\left[\frac{1}{nm}\right],Ha=5,\frac{\rho_s}{\rho_f}=2000,\psi_w=-50[m\mathrm{V}],E_r=30\left[\frac{\mathrm{kV}}{m}\right]\right)$$

the optimal normalized velocity is not determined by choosing specific wedge semi angle but may vary along the course and optimal value may be achieved in some point over the tangential direction for other wedge semi angle than initially specified as appear in Fig. 11. The last case that will be brought here concerns the effect of friction coefficient (m) variation on the normalized velocity profile for different values of wedge semi angle (α) with the following parameters choice

$$\left(\phi=0.02,\mathrm{Re}=250,\kappa=1000\left[\frac{1}{nm}\right],Ha=50,\ \frac{\rho_s}{\rho_f}=10^4,\psi_w=-50[m\mathrm{V}],E_r=150\left[\frac{\mathrm{kV}}{m}\right]\right)$$

. One can infer from the friction coefficient variation that the difference between the normalized velocity profiles for different values of α is decreased as long as the friction coefficient is increased as presented in Fig. 12 (a-d). Moreover, choosing large values of m leads to profiles convergence. For instance, in case where the friction coefficient represents "infinity" ($m=10^6$) the profiles are coincided as appear in Fig. 12. (e).

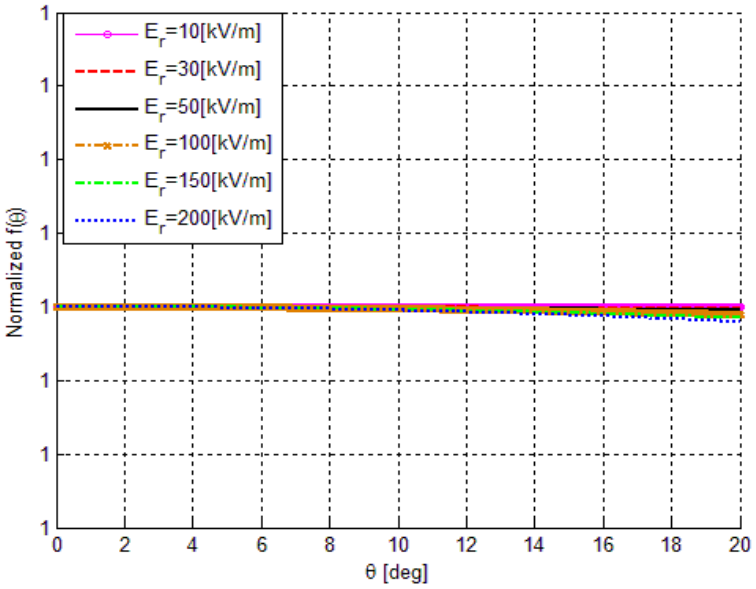

Fig. 10. Normalized velocity $f(\theta)$ for various values of the electrical field (E_r).

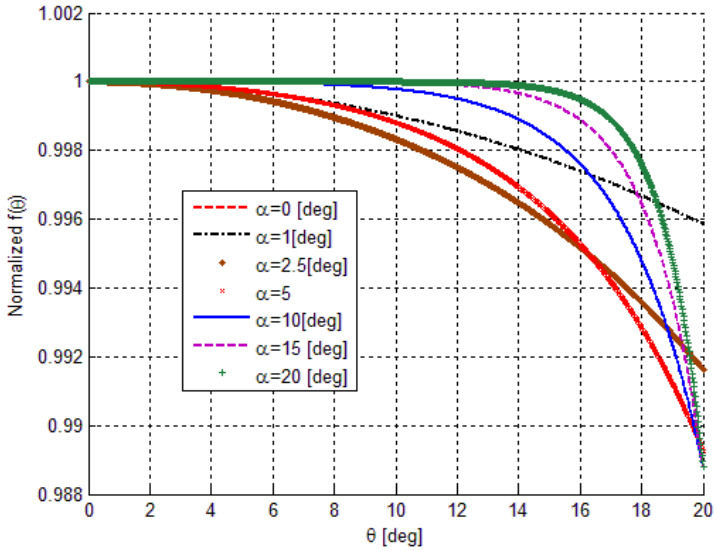

Fig. 11. Normalized velocity $f(\theta)$ for various values of the wedge semi angle (α).

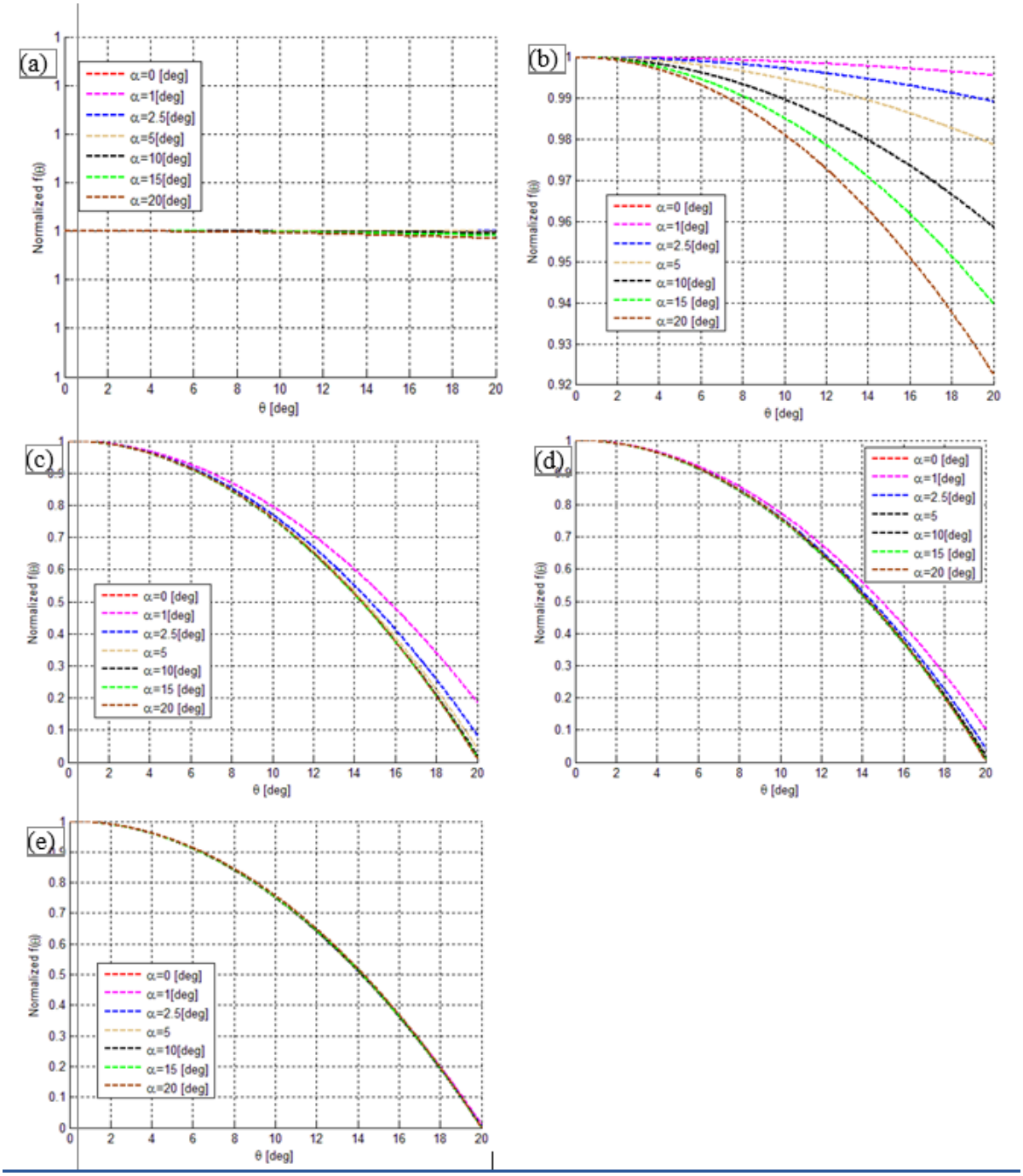

Fig. 12. Normalized velocity $f(\theta)$ for various values of the wedge semi angle (α) in accordance to the following cases:

a. $m=0$. **b.** $m=0.5$. **c.** $m=500$. **d.** $m=10^4$. **e.** $m=10^6$.

5. CONCLUSIONS

In this essay, a model of combined MHD and electroosmotic Jeffery–Hamel flow of nano fluid type inside a wedge (inclined walls) with non-linear viscosity and wall friction was derived and expressed by one nonlinear ordinary differential equation with appropriate boundary conditions based on similarity relations. The obtained equation can be solved analytically by assuming that $f^2 \square f$ and $0<\theta\le 20^0$. Moreover, the obtained analytic solution was compared to simple parabolic approximation while excellent agreement was found. Although it was found that in case where more effects are gradually being considered, a slight difference is emerged, but the most dramatic change between solutions occurs when solid to fluid ratio ρ_s / ρ_f gets significant value. In addition, literature results were also being compared, while solutions were

found to have suitable match in the quantitatively and qualitatively aspects.

Moreover, analytical solution parametric investigation was performed for specific parameters choice. It was found that the normalized velocity (f) was decreased gradually with the tangential direction progress and/or with friction coefficient (m) increase. However, the normalized velocity profile gets higher values as long as the solid to fluid ratio ρ_s / ρ_f increases. Additionally, Reynolds (Re), Hartmann (Ha) and solid volume fraction coefficient (ϕ) increase (separately or all together) have raised the normalized velocity function values.

Finally, three unprevail distinguished cases were introduced to understand flow complexity. It was found that electrical field magnitude effect is being significant, especially for small friction coefficient values and for high wedge semi angle. In addition, the combination between small friction coefficient values including small parameter flow values (Re and Ha numbers) and high electrically field may lead to un-optimized course of normalized velocity profile. The last case that was examined deals with friction coefficient (m) variation effect on the normalized velocity profile for different values of wedge semi angle (α) with high electric field for specific parameters choice. One can infer from the variation of friction coefficient that the difference between the normalized velocity profiles for different values of α decreases as long as the friction coefficient increases. Moreover, choosing large values of m leads to profiles convergence such as in case where the friction coefficient represents "infinity" ($m=10^6$) the profiles are coincided.

REFERENCES

1. Rice C. L., Whitehead R., 1965, Electrokinetic Flow in a Narrow Cylindrical, ***The Journal of Physical Chemistry***, **69**, 11, 4017-4024
2. Sørensen T. S., Koefoed J., 1974, Electrokinetic Flow in a Narrow Cylindrical Capillary, ***J. Chem. Soc. Faraday Trans.*** 2(70): 665-675
3. Levine S., Marriott J. R., Robinson K., 1975, Theory of electrokinetic flow in a narrow parallel-plate channel, ***J. Chem. Soc. Faraday Trans.*** 2(71): 1-11
4. Pu Q., Yun Q. J., Temkin H., Liu S., 2004, Ion Enrichment and Ion-Depletion Effect of Nanochannel Structures, **Nano Letters,** 4(6): 1099-1103
5. Plecis A., Schoch R. B., Renaud P., 2005, Ionic Transport Phenomena in Nanofluidics: Experimental and Theoretical Study of the Exclusion-Enrichment Effect on a Chip. ***Nano Lett.,*** 5(6): 1147–1155
6. Byun C. K.., Wang X., Pu Q., Liu S., 2007, An Electroosmosis-Based Nanopipettor, ***Anal Chem.,*** 79(10): 3862–3866
7. Berrouche Y., Avenas Y., Schaeffer C., Wang P., Chang H. C., 2008, Optimization of High Flow Rate Nanoporous Electroosmotic Pump, *ASME. **J. Fluids Eng***. 130(8): 081604-081604-7
8. Chen L., Li Q., Lee s., Choo J., 2008, Development of an Electroosmotic Pump Using Nanosilica Particle Packed Capillary**. *Sensors Journal*, *IEEE*,** 8(5): 488-494.
9. Chen Y. F., M. C. Li, Y. H. Hu, W. J. Chang and C. C. Wang, 2008, Low-voltage electroosmotic pumping using porous anodic alumina membranes, ***Microfluid Nanofluid***, 5: 235–244
10. Seiler M., Kirby B., Computational simulation of electrohydrodynamic systems pertaining to micro and nano scale fluid flow phenomenon, Excerpt from the Proceedings of the COMSOL Conference 2008 Boston
11. Ai Y., Zhang M., Joo S. W., Cheney M. A., Qian S., 2010, Effects of Electroosmotic Flow on Ionic Current Rectification in Conical Nanopores, ***J. Phys. Chem. C***, 114 (9): 3883–3890
12. Piruska A., Gong M., Sweedler J. V., Bohn P. W., 2010, Nanofluidics in chemical analysis, **Chem. Soc. Rev.**, 39: 1060-1072
13. Aparajita A., Satapathy A. K., 2012, Numerical analysis of heat transfer characteristics of combined electroosmotic and pressure-driven fully developed flow of power law nanofluids in microchannels, 3rd European Conference on Microfluidics - 2012 - Heidelberg, Germany, 1-10
14. Avsec J., 2012, Electrokinetic and nanofluid slip flow in rectangular and circular microchannels regarding constant heat flux, *Nanotechnology* (*IEEE-NANO*), 12th IEEE Conference on Nanotechnology, 1-6
15. Imani A. A., Rostamian Y., Ganji D. D., Rokni H. B., 2012, Analytical Investigation of Jeffery-Hamel Flow with High Magnetic Field and Nano Particle by RVIM. ***IJE TRANSACTIONS C: Aspects***, 25(3): 249-256
16. Kurtoğlu E., Bilgin A., Şeşen M., Mısırlıoğlu B., Yıldız M., Funda H., Acar Y., Kosar A., 2012, Ferrofluid actuation with varying magnetic fields for micropumping applications, **Microfluidics and Nanofluidics,** 13(4): 683-694
17. Ahmed S., Mahdy A., 2012, Natural Convection Flow and Heat Transfer Enhancement of a Nanofluid past a Truncated Cone with Magnetic Field Effect. ***World Journal of Mechanics***, 2(5): 272-279
18. Khidir A. A., 2013, A New Spectral-Homotopy Perturbation Method and Its Application to Jeffery-Hamel Nanofluid Flow with High Magnetic Field, ***Journal of Computational Methods in Physics***, 1- 10
19. Sadoughi K., Hosseini M., Shakeri F., Azimi M., 2013, Analytical Simulation of MHD Nanofluid Flow over the Horizontal Plate, ***Frontiers in Aerospace Engineering***, 2(4): 242 – 246
20. Umavathi J. C., Shekar M., 2013, Effect of MHD on Jeffery-Hamel Flow in Nanofluids by Differential Transform Method***, Int. Journal of Engineering Research and Applications,*** 3(5): 953-962.
21. Ganji D. D., Azimi M., 2013, Application of DTM on MHD Jeffery Hamel problem with nanoparticles, **U.P.B. Sci Bull. Ser. A**, 75: 223 – 230

22. Hatami M., Sheikholeslami M., Hosseini M., Ganji D. D., 2014, Analytical investigation of MHD nanofluid flow in non-parallel walls, **Journal of Molecular Liquids, 194:** 251-259
23. Mao M., Sherwood J. D., Ghosal S., 2014, Electroosmotic flow through a nanopore***, J. Fluid Mech***., 749: 1 – 16
24. Alam M. S., and Khan M. A. H., 2014, Analysis of MHD Jeffery-Hamel flow with nanoparticle by Hermite- Padé approximation, ***Journal of Advanced Science and Engineering Research***, 4(2): 103-117
25. Nayak A. K., 2014, Enhancement of flow mixing in micro and nano. **ANZIAM J. EMAC2013**, 55: C47-C63
26. Deng X. L., Takami T., Son J. W., Kang E. J., Kawai T., Park B. H., 2014, Effect of concentration gradient on ionic current rectification in polyethyleneimine modified glass nano-pipettes. ***Scientific Reports*** 4, 4005, 1-8
27. Mustafa M., Khan J. A., Hayat T., Alsaedi A., 2015, Analytical and numerical solutions for axisymmetric flow of nanofluid due to non-linearly stretching sheet, ***International Journal of Non-Linear Mechanics***, 71: 22-29
28. Ganguly S., Sarkar S., Hota T. K., Mishra M., 2015, Thermally developing combined electroosmotic and pressure-driven flow of nanofluids in a microchannel under the effect of magnetic field, **Chemical Engineering Science,** 126:, 10-21
29. Lin D. H., Lin C. Y., Tseng S., Hsu J. P., 2015, Influence of electroosmotic flow on the ionic current rectification in a pH-regulated, conical nanopore, **Nanoscale.**,**7**: 14023–14031
30. Laohakunakorn N., Keyser U. F., 2015, Electroosmotic flow rectification in conical nanopores, ***Nanotechnology,*** 26: 1-9
31. Moradi A., Alsaedi A., Hayat T., 2015, Investigation of Heat Transfer and Viscous Dissipation, ***Thermal Science,*** 19(2): 563-578
32. Nagler J., Durban D., Khosid S., 2013, On Planar Radial Flow with non-Uniform Viscosity and Wall Friction Without Inertia Effect, Technion – Israel Institute of Technology, Master Project.
33. Bird C., Breward C. J. W., Dellar P., Edwards C. M., Kaouri K., Richardson G., Wilson S. K., 2002, Mathematical modeling of pipe-flow and extrusion of composite materials. Study Group Report
34. Sadeghy K., Khabazi N., Taghavi S. M., 2007, Magnetohydrodynamic (MHD) Flows of Viscoelastic Fluids in Converging/Diverging Channels, ***International Journal of Engineering Science***,45(11): 923-938
35. Thess A., Votyakov E., Kolesnikov Y., 2006, Lorentz Force Velocimetry***, Phys. Rev. Lett***., 96: 164501-1 – 4
36. Sarkar S., Ganguly S., 2015, Fully developed thermal transport in combined pressure and electroosmotically driven flow of nanofluid in a microchannel under the effect of a magnetic field, ***Microfluidics and Nanofluidics, 18(4):*** 623-636
37. Membrado M., Pacheco A. F., 2011, Equations in Curvilinear Coordinates for Fluids With non-Constant Viscosity, ***Latin-American Journal of Physics Education***, 5(4): 702-708
38. Sherwood J. D., Durban D., 1996, Squeeze Flow of a Power law Viscoplastic Solid, ***J. Non-Newtonian Fluid Mech.,*** 62: 35–54.
39. Dib, A., Haiahem, A., Bou-said, B., 2014, An Analytical Solution of the MHD Jeffery–Hamel Flow by the Modified Adomian Decomposition Method, ***Computers & Fluids***, 102: 111-115